Forest Chemicals Revew
www.forestchemicalsreview.com
ISSN: 1520-0191
July-August 2021 Page No. 728-746
Article History: Received: 12 May 2021 Revised: 25 June 2021 Accepted: 22 July 2021 Publication: 31 August 2021

Study on the Control of Buffeting Noise of a Car Driving with the Front Side Window Open

Youbin Wang[1,*], Xutao Yu [2]
[1]School of Mechanical Engineering, Nanjing Institute of Technology, Nanjing, China
[2]Pan Asia Technical Automotive Center, Shanghai, China
*Corresponding Author.

Abstract:

In order to reduce buffeting noise in the cab when a car was driving with the front side window is opener, the large eddy simulation method is used to simulate the flow around the car. Combined with the solution of buffeting noise of the side window, the influence factors of the rear-view mirror wake vortex of the buffeting noise are studied and the influence mechanism is analyzed. Then, to reduce the large buffeting noise of the vehicle, the corresponding control measures are proposed based on the destruction of the free shear layer and its vortex structure. By adding two kinds of deflectors on the triangle window area, the level of buffeting noise in the cab is reduced, and the reason of the reduction of buffeting noise is analyzed.

Keywords*: Automotive aerodynamics, Buffeting noise, Computational fluid dynamics, Large eddy simulation.*

I. INTRODUCTION

Most vehicles have the problem of buffeting noise, when, driving with sunroof or side window open. Vehicle buffeting noise is a kind of low-frequency (below 20Hz) high-intensity (100dB) noise [1], which is hard to be detected by human ear, but it can be obviously felt its existence. Buffeting noise seriously affects the quality of vehicle NVH (Noise, Vibration, Harshness) and the user experience of drivers and passengers. It is very easy to produce driving fatigue under the buffeting noise for a long time. It can cause serious safety risks for the low-frequency and high-intensity pressure pulsation even produces on the vehicle structure Fatigue damage [2, 3]. When the car is driving with windows open, the fluid inside and outside the car will interact. Due to the good sealing performance of the car body, the pressure pulsation in the car is intense and causes strong low-frequency noise. The pulsation pressure acts on the human ear, causing discomfort to the drivers and passengers in the compartment [4].

Forest Chemicals Revew
www.forestchemicalsreview.com
ISSN: 1520-0191
July-August 2021 Page No. 728-746
Article History: Received: 12 May 2021 Revised: 25 June 2021 Accepted: 22 July 2021 Publication: 31 August 2021

According to the research of foreign scholars such as Didyk, the pneumatic pressure pulsation with small amplitude will change the shape of the relaxation part of the tympanic membrane, resulting in human discomfort [5]. In addition to low-frequency pulsation pressure, some vehicles have the problem of high-frequency resonance noise, which will lead to serious roar in the passenger compartment. Vehicle buffeting noise is one of the aerodynamic noise problems that consumers complain about, which seriously restricts the performance of automobile products. Therefore, it is meaningful to study the generation mechanism and influencing factors of vehicle buffeting noise and put forward corresponding control strategies. The vehicle buffeting noise can be caused when sunroof or side window is opened. Many scholars have carried out a detailed study on the vehicle buffeting noise through experiments and numerical simulation.

In the 1960s, the engineers of Ford Motor Company, Bodger and Jones, studied the buffeting noise of the rear side window of the bus by experiments. They found that at a certain speed, there would be an uncomfortable pressure pulse in the car, which was called "wind throb". At the same time, they proposed the method of reducing the buffeting noise [6]. In 2009, Huang Lei of Shanghai Jiaotong University carried out the research on the buffeting noise, studied the mechanism of the buffeting noise of sunroof, introduced two control methods to reduce buffeting noise [7]. In 2010, Kangning studied the buffeting noise of the simplified golf car with sunroof. With the sunroof position moving backward, the sound pressure level at the monitoring point gradually decreased, and the ideal sunroof size and installation position were determined [8]. In 2010, Wang Yiping of Hunan University simulated the buffeting noise of automobile sunroof, revealed that vortex shedding at the opening is the main source of buffeting noise, and proposed that reasonable installation of guide plate and reasonable open of sunroof can reduce buffeting noise [9]. In 2011, Hu Yatao et al. of Huazhong University of science and technology calculated the buffeting noise with a 1:5 simplified model. They analyzed the flow field structure and the causes of the buffeting noise. It was found that with the increase of the velocity, the broadband noise gradually increased [10]. In 2012, Wang Yiping of Hunan University conducted wind-induced vibration simulation analysis on the basis of experiments, and found that the buffeting noise of the rear side window was higher than that of the front side window, and studied the relationship between buffeting noise and vehicle speed, vehicle volume, side window opening position and side window opening number. The maximum noise reduction of the rear side window is 9dB through the way of notching in the B-pillar area and adding a pillar to the rear side window [11]. In 2013, Chen Zhifu et al. of Hunan University used large eddy simulation method to carry out numerical simulation on the wind vibration characteristics of sunroof. They found the influence rule of the velocity on the buffeting noise, and obtained the conclusion that the buffeting noise in the rear edge of sunroof and near the floor is the largest [12]. In 2013, Ganapathi Balasubramanian et al. simulated the

Forest Chemicals Revew
www.forestchemicalsreview.com
ISSN: 1520-0191
July-August 2021 Page No. 728-746
Article History: Received: 12 May 2021 Revised: 25 June 2021 Accepted: 22 July 2021 Publication: 31 August 2021

buffeting noise and rearview mirror aerodynamic noise in the early stage of vehicle development, and compared the impact of different rearview mirrors on the front side window buffeting noise [13]. In 2014, Yang Zhendong of Hunan University used large eddy simulation to simulate the buffeting noise of vehicle sunroof with guide plate. He optimized the installation angle, slot width, slot depth and other parameters of slotted guide plate, and achieved good noise reduction effect [14]. In 2015, Nicholas Oettle and others of Jaguar Land Rover simulated the wide-band noise under the opening of the sunroof, and concluded that the wide-band noise of the sunroof comes from the turbulence in the sunroof area. The impact of the free shear layer and the vortex on the rear edge of the sunroof are the causes of the noise [15]. In 2016, Farokh Kavarana et al. of Nissan Automotive Technology Center designed an airfoil section deflector to control the buffeting noise of the sunroof, proving that this control method can make the free shear layer more stable, and can effectively reduce the buffeting noise [16].In 2017, Zhang Qidong and Gu Zhengqi of Hunan University studied the influence of different opening combinations of side windows of high-speed vehicles on the characteristics of buffeting noise, and put forward reasonable opening suggestions [17].In 2019, Chen Qingbin and others studied the control measures of buffeting noise of passenger cars, optimized the spoiler at the front edge of the sunroof, and achieved good noise reduction effect [18]. In 2019, Dunai L. et al evaluated the buffeting noise effect in a BMW 530d model vehicle in an outdoors highway at different speeds and demonstrated that the buffeting-noise effect is independent from the listener position [19]. In 2019, Chen Z. et al proposed a modified LRN CLES model and indicated that the modified LRN CLES model simulates the vehicle window buffeting noise greater than commonly used models [20]. In 2019, Yin S. et al verified that LES method was employed to calculate automobile side-window buffeting noise by wind tunnel experiments and studied the influence of driving velocity and window opening degree on wind buffeting noise characteristics [21]. In 2020, Zhang Q. et al constructed a sub-cavity by attaching an inclined baffle near the leading edge of the sunroof to suppress the buffeting SPL at 70 kph and the reduction of sunroof buffeting reached 33.6 dB by optimizing the size of the sub-cavity [22]. In 2020, Kim H. et al studied the flow features and noise contribution of two types of noise reduction treatments rounded and chamfered edges of a rectangular cavity and investigated the effects of the rounded cavity edges on the flow and noise of a simplified high-speed train pantograph [23]. In 2021, Wang Q. et al reviewed the classification, evaluation and research methods of wind noise, as well as the characteristics and control methods of wind buffeting vibration noise [24]. In 2021, Tang R. et al analyzed the characteristics of the sunroof buffeting noise of a commercial vehicle model and the SPL of the sunroof buffeting noise was reduced by 6.7 dB and the wind resistance coefficient was reduced by 1.55% by optimizing the sun visors and roof domes [25]. In 2021, Li S. et al reduced the aerodynamic resistance coefficient of the commercial vehicle by 2.07% and the SPL of sunroof buffeting noise by 18.3 dB by optimizing the sun visor installation angle and roof dome shape [26]. In 2021, Yu A. et

Forest Chemicals Revew
www.forestchemicalsreview.com
ISSN: 1520-0191
July-August 2021 Page No. 728-746
Article History: Received: 12 May 2021 Revised: 25 June 2021 Accepted: 22 July 2021 Publication: 31 August 2021

al proposed two improved models, called ILRN k-epsilon and DES-ILRN, and the accuracy of ILRN and DES-ILRN in calculating wind buffeting noise of a real vehicle is validated by experiment [27]. In 2021, Zhang Y. et al studied the effects of incoming boundary layer thickness and shapes on cavity buffeting noise characteristics based on Omega vortex identification method and WMLES turbulence model [28].

In summary, the sunroof buffeting noise has been effectively controlled by adding deflectors and other devices, and has been applied in automotive products. The flow characteristics of the side window area are more complex. At present, the research on the suppression of the buffeting noise on the side window area is most about the combination of window opening and adding additional devices at the B-pillar to reduce the buffeting noise of the rear side window. In this paper, the numerical simulation method is used to study the flow characteristics inside and outside the passenger compartment of the whole vehicle and its influence mechanism on the buffeting noise. Furthermore, the control method of buffeting noise of front side window is put forward, which provides theoretical basis for subsequent research and engineering application.

II. NUMERICAL COMPUTATION SCHEME

2.1 Large Eddy Simulation

The LES method is a high-precision, high-efficiency numerical simulation method, which is one of the main methods currently used in the CFD field between direct numerical simulation and Reynolds time-average method. The results show that LES can better capture the aerodynamic noise characteristics compared to the two other techniques [29]. First, incompressible Navier–Stokes (N–S) equation is filtered before the large-scale vortexes are preserved and solved by the transient N–S equation according to the theory of LES. Second, the sublattice model is used to determine the effect of small-scale vortex on the large-scale one and modify the filtered N–S equations in the form of additional stress terms [30].

2.2 Lighthill Acoustic Wave Equation

Accurate understanding of the fluid sound generation mechanism has important theoretical significance for the analysis of the characteristics of wind vibration noise of automobile side windows. Lighthill acoustic wave equation is a widely used basic theoretical model in aeroacoustics, the expression is [31]:

$$\frac{\partial^2 \rho'}{\partial t^2} - c_0^2 \nabla^2 \rho' = \frac{\partial^2 T_{ij}}{\partial x_i \partial x_j} \tag{1}$$

Forest Chemicals Revew
www.forestchemicalsreview.com
ISSN: 1520-0191
July-August 2021 Page No. 728-746
Article History: Received: 12 May 2021 Revised: 25 June 2021 Accepted: 22 July 2021 Publication: 31 August 2021

$$T_{ij} = \rho u_i u_j + [(p - p_0) - c_0^2(\rho - \rho_0)]\delta_{ij} \quad (2)$$

where T_{ij} is Lighthill stress tensor; $(p\text{-}p_0)$ is pressure pulsation; $(\rho\text{-}\rho_0)$is fluctuation of fluid density; δ_{ij} is unit tensor; c_0 is the speed of sound.

Large eddy simulation can be used to solve compressible fluid to capture both flow disturbance and pressure wave disturbance.The sound pressure signal of the monitoring point in time domain is transformed into the sound pressure level spectrum curve by fast Fourier transform (FFT).

$$SPL = 20\lg\frac{p'}{p_{ref}} \quad (3)$$

where p' is the pulsating pressure; pref is the reference pressure value ;and pref=2×10−5 Pa.

III. CALCULATION SETTINGS

3.1 Computation Model and Domains

The numerical simulation model is a sedan, there is a driver dummy model in the cab, and the base of the rearview mirror is installed on the door. Details such as door handle, wiper and smooth chassis are ignored and the interior decoration is simplified accordingly. The model is shown in figure 1 and figure 2 is the three views of the interior decoration structure. In this part, the wind vibration noise simulation of the side window selects the fully open condition of the driver's left front window.

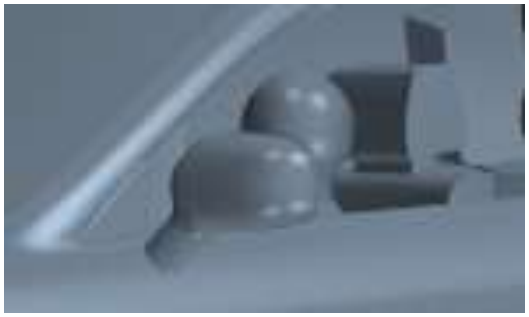

Fig 1: geometry model

Forest Chemicals Revew
www.forestchemicalsreview.com
ISSN: 1520-0191
July-August 2021 Page No. 728-746
Article History: Received: 12 May 2021 Revised: 25 June 2021 Accepted: 22 July 2021 Publication: 31 August 2021

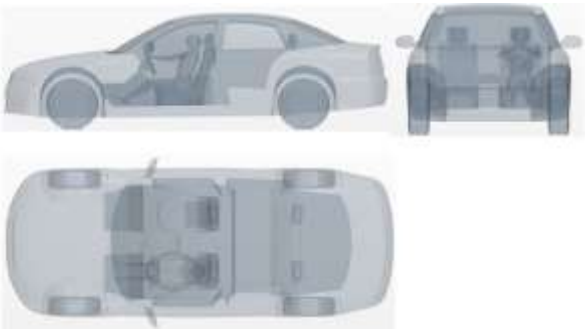

Fig 2: interior structure of the model

The computational domain setting is shown in Figure 3, where the vehicle height (H), length (L), and width (W) are 1400, 4620, and 2040 mm, respectively. The size of the whole calculation field is set to be 11 times the model length L in the length direction, 3 times the model length L in the distance from the entrance of the calculation field to the front of the model, 7 times the model length L in the distance from the back of the model to the exit of the calculation field, 5 times the height of the model H in the height of the calculation field, and 7 times the width of the model W in the width of the calculation field.

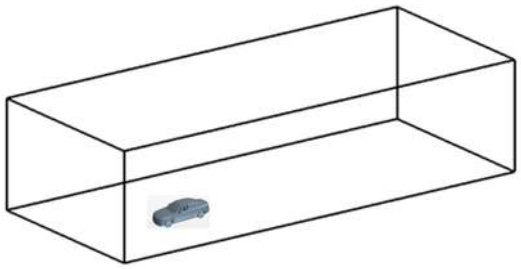

Fig 3: computational domain of flow field

3.2 Grid Division

The face mesh uses a triangular mesh to accurately capture the shape and improve the quality of the mesh. The critical flow areas, such as A-pillars, rear-view mirrors, window areas, large area of the front curvature, and wake area, use small-grid scales. In other areas, the surface grid scale increases gradually to ensure that the surface mesh changes smoothly. The volume mesh uses unstructured tetrahedral mesh. Three volume grid encryption areas are set in the computational domain to accurately simulate the external flow field of the car. The encryption area is set separately in the wake area of the mirror and in the opening area of the

Forest Chemicals Revew
www.forestchemicalsreview.com
ISSN: 1520-0191
July-August 2021 Page No. 728-746
Article History: Received: 12 May 2021 Revised: 25 June 2021 Accepted: 22 July 2021 Publication: 31 August 2021

side window to accurately capture the side window flow information. An independent encryption zone is set inside the cavity to capture the flow within the cavity. For the volume grid, a smooth transition of the grid size should be ensured. The surface grid is presented in Figure 4, and the volume grid and encryption area are shown in Figure 5.

The airflow generates a boundary layer attached to the surface of the car due to viscosity. Ten layers of boundary layer grid, combined with the low Reynolds number turbulence model, are set to accurately capture the flow on the wall surface, as shown in Figure 5. Finally, the volume mesh of the model is approximately 36 million.

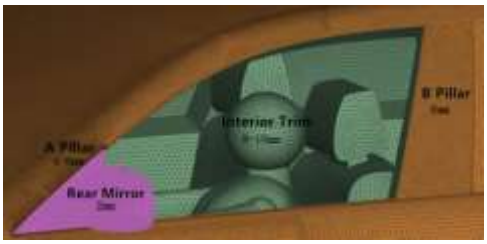

Fig 4: surface grid

Fig 5: the mesh distribution and boundary layer

3.3 Boundary Condition Settings

The boundary conditions used in this section are shown in Table I.

TABLE I. Boundary condition setting

BOUNDARY CONDITION OF COMPUTATIONAL DOMAIN	SETTING OF BOUNDARY DOMAIN
INLET	Inlet speed V_x=22.22m/s, V_y=0, V_z=0 Turbulence characteristic speed=0.07 m; turbulence intensity=0.027

Forest Chemicals Revew
www.forestchemicalsreview.com
ISSN: 1520-0191
July-August 2021 Page No. 728-746
Article History: Received: 12 May 2021 Revised: 25 June 2021 Accepted: 22 July 2021 Publication: 31 August 2021

OUTLET	Pressure outlet=101325 Pa
GROUND OF COMPUTATIONAL DOMAIN	Slip wall
SIDE AND TOP	Symmetrical wall

The steady-state simulation is the initial condition for transient simulation, and its solver settings are shown in Table II.

TABLE II. The steady-state solver settings

SETTING ITEMS	SETTING
SOLVER	Pressure Based
TIME	Steady
AIR	Ideal-gas
TURBULENCE MODEL	$SST\ k-\omega$
PRESSURE-VELOCITY COUPLING	SIMPLE
PRESSURE DISCRETIZATION	Second Order
MOMENTUM DISCRETIZATION	Second Order Upwind
TURBULENT KINETIC ENERGY DISCRETIZATION	Second Order Upwind
TURBULENT DISSIPATION RATE DISCRETIZATION	Second Order Upwind
ENERGY DISSIPATION	Second Order Upwind

The setting of the transient simulation solver is shown in Table III.

TABLE III. The setting of the transient simulation solver

SETTING ITEMS	SETTING
SOLVER	Pressure Based
TIME	Unsteady,2nd order

Forest Chemicals Revew
www.forestchemicalsreview.com
ISSN: 1520-0191
July-August 2021 Page No. 728-746
Article History: Received: 12 May 2021 Revised: 25 June 2021 Accepted: 22 July 2021 Publication: 31 August 2021

△T	0.002s
AIR	Ideal-gas
TURBULENCE MODEL	LES
PRESSURE-VELOCITY COUPLING	SIMPLE
PRESSURE DISCRETIZATION	Second Order
MOMENTUM DISCRETIZATION	Second Order Upwind
ENERGY DISSIPATION	Second Order Upwind

The transient state is calculated for a total of 3 seconds, and the time-domain pressure pulsation curve is obtained. After taking the stable data for a period of 2 seconds, FFT is performed to obtain the spectrum diagram of the sound pressure level curve.

3.4 Monitoring point setting

A total of four monitoring points are arranged in the crew cabin, as shown in Figure 6, which are located on the outer ear side of the four crew positions, respectively, the left front monitoring point (1.4799, -0.4335, 0.7719); right front monitoring point (1.4799, 0.4335, 0.772); left rear monitoring point (2.4799, -0.4335, 0.7719); right rear monitoring point (2.4799, 0.4335, 0.772), the unit of the above data is m.

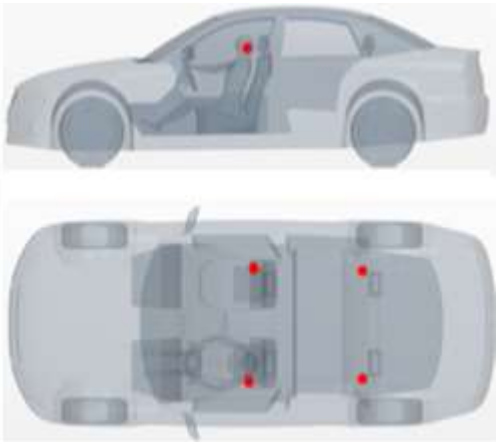

Figure 6: schematic diagram of monitoring point location

IV. COMPUTATIONAL RESULT ANALYSIS

Forest Chemicals Revew
www.forestchemicalsreview.com
ISSN: 1520-0191
July-August 2021 Page No. 728-746
Article History: Received: 12 May 2021 Revised: 25 June 2021 Accepted: 22 July 2021 Publication: 31 August 2021

4.1 Analysis of wind vibration characteristics of front side window

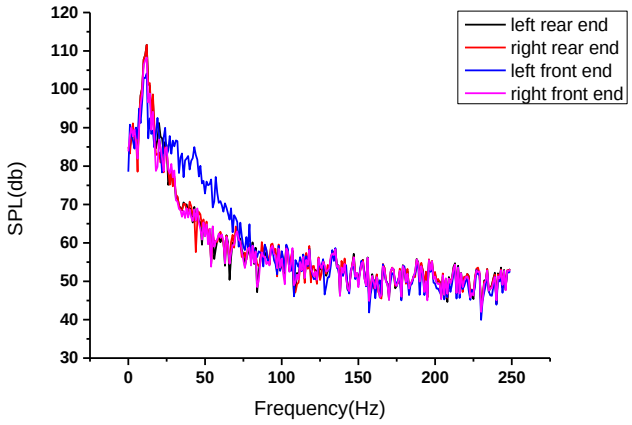

Figure 7: SPL at each monitoring point

It can be seen from Figure 7 that the maximum value of the first-order peak value of the sound pressure level spectrum diagram of this model is 112dB, which indicates the occurrence of side window buffeting, and the frequency is 15Hz. Except for the accident at the window opening side (the front left monitoring point), the monitoring data at other locations is almost the same.

The characteristics of wind vibration are analyzed through the flow state of airflow near the front side window .The Q-criterion is used to define the vortex isosurface, and the Q>0 area can be used to determine the presence of a vortex. The envelope area defines the distribution of the vortex cores. The Q value in Figure 8 is 104 s−2. The color rendering is in the form of a pressure cloud diagram, and the vortex isosurface can reflect the form of a vortex structure in space.

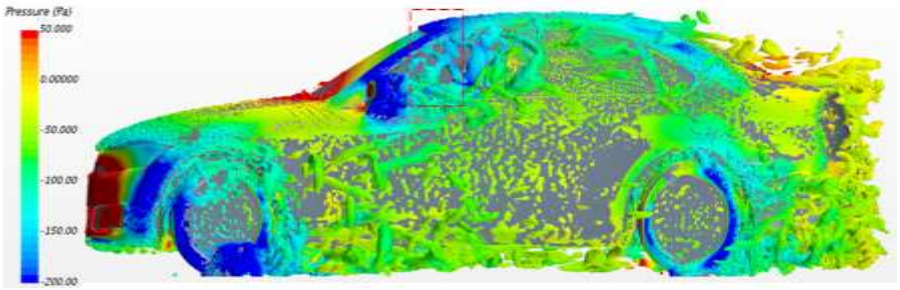

Forest Chemicals Revew
www.forestchemicalsreview.com
ISSN: 1520-0191
July-August 2021 Page No. 728-746
Article History: Received: 12 May 2021 Revised: 25 June 2021 Accepted: 22 July 2021 Publication: 31 August 2021

Figure 8: Q isosurface cloud image with front window open

It can be found from Figure 8 that there is a strong vortex structure in the front window area.The trailing vortex of the rearview mirror is located at a lower position, and the overlap area of the vortex formed with the free shear layer is relatively small, which has little influence on the free shear layer. Therefore, an obvious free shear layer shedding vortex can be observed in the lower part of the front window.

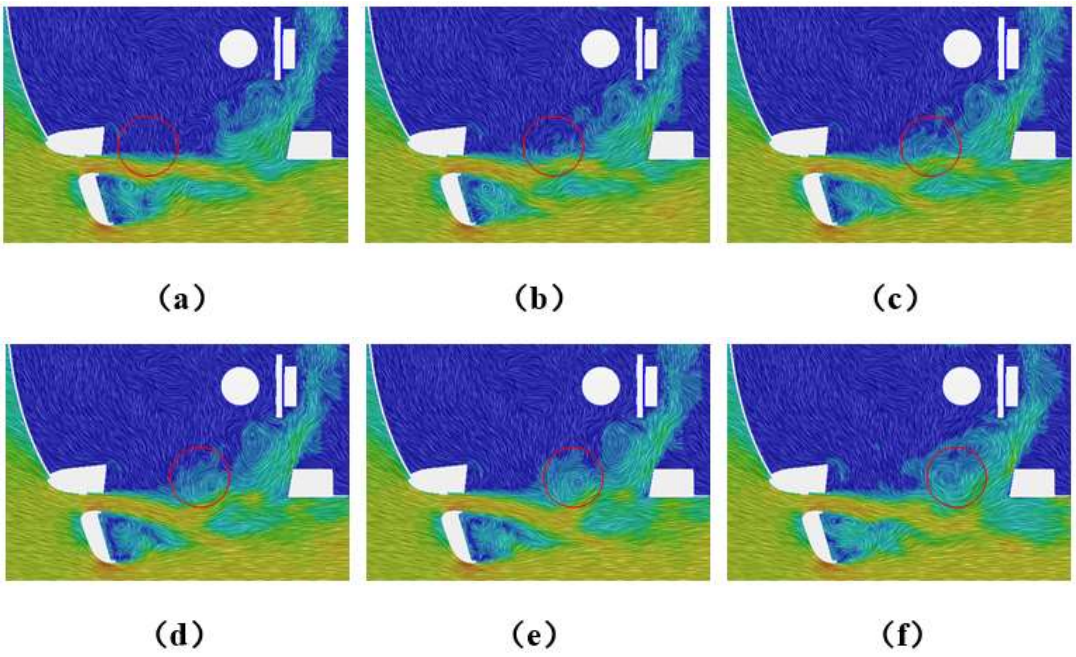

Figure 9: evolution process of free shear layer vortex in front window

As can be seen from Figure 9, the trailing vortex of the rear-view mirror has a certain influence on the movement and development of the free shear layer and its vortex. (a) The tail of the free shear layer is obviously oscillating, causing disturbance at the front of the front side window and starting to form vortices. (b) As the vortex structure continues to develop, the wake vortex of the rear-view mirror sways to the passenger compartment side. And the wake vortex of the rear-view mirror interferes with the free shear layer and its vortex. (c)The vortex structure continues to develop and the interference effect of the rear-view mirror wake vortex is strengthened. (d)The vortex structure moves backward and increases continuously. With the movement of the trailing vortex in the rear-view mirror, the distance gradually increases and the influence gradually weakens. (e) The vortex structure continues to move backward and develops continuously, while the wake vortex gradually moves backward and the influence is

Forest Chemicals Revew
www.forestchemicalsreview.com
ISSN: 1520-0191
July-August 2021 Page No. 728-746
Article History: Received: 12 May 2021 Revised: 25 June 2021 Accepted: 22 July 2021 Publication: 31 August 2021

further weakened. (f)The vortex invades into the cavity, and the tail vortex of the rear-view mirror separates from the B-pillar.

In the evolution process, because the rear-view mirror tail vortex is relatively far away from the free shear layer, the free shear layer is less affected by the negative pressure region of the rear-view mirror tail vortex, and the overall deviation is not obvious. The rear-view mirror tail vortex has a certain restraining effect on the development of the free shear layer and its vortex, but its influence is relatively weak.

V. CONTROL SCHEME

5.1 Addition of Vertical Diversion Slice

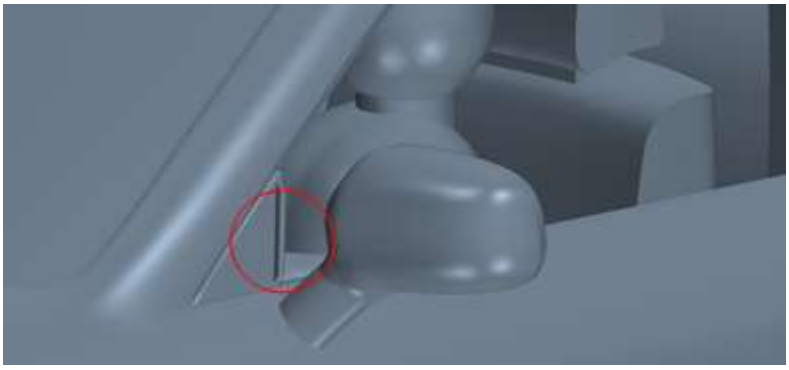

Fig 10: a vertical backflow slice to the position of the triangular window

In the position of the triangular window, adding vertical diversion slice as shown in Figure 10. It can be found from the previous simulation results that, at the simulation speed of this model, the buffeting noise data of all the monitoring points in the crew cabin except the opened side are basically the same. Therefore, the sound pressure level spectrum curves of the monitoring points in the crew cabin at the left rear side and the monitoring points at the left front window side are selected in this part for analysis.

Forest Chemicals Revew
www.forestchemicalsreview.com
ISSN: 1520-0191
July-August 2021 Page No. 728-746
Article History: Received: 12 May 2021 Revised: 25 June 2021 Accepted: 22 July 2021 Publication: 31 August 2021

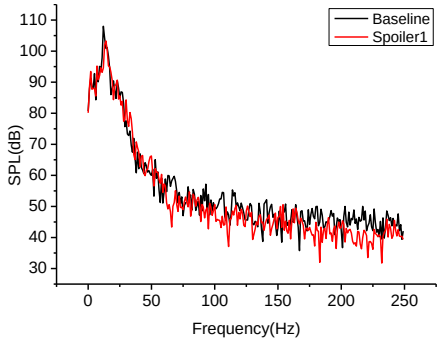

Figure 11: SPL of left rear monitoring point

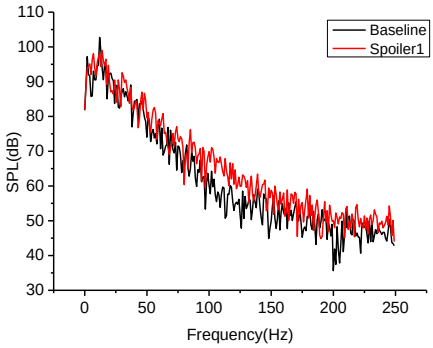

Figure 12: SPL of Left front monitoring point

Figures 11 and 12 indicate that adding a vertical diversion slice has a significant restraining effect on the buffeting noise in the vehicle when the front left window is opened. The left rear monitoring point can reduce noise by 4.8 dB, whereas the left front monitoring point reduces noise by 3.75 dB. These values show evident noise reduction.

Forest Chemicals Revew
www.forestchemicalsreview.com
ISSN: 1520-0191
July-August 2021 Page No. 728-746
Article History: Received: 12 May 2021 Revised: 25 June 2021 Accepted: 22 July 2021 Publication: 31 August 2021

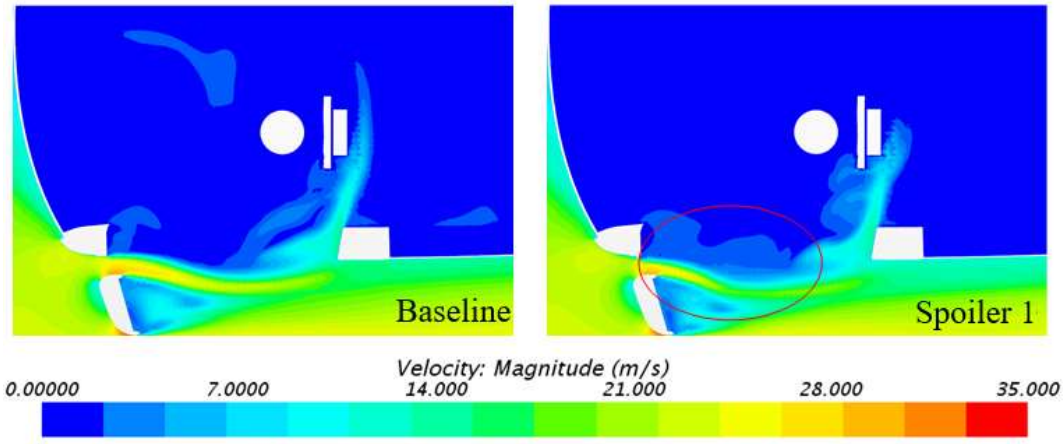

Fig 13: comparison of scalar plots of Z=0.7m plane velocity

The formation of the shear layer is caused by the velocity difference of the fluid. In Figure. 13, it can be found that the velocity in the cavity of the left basic model is significantly lower, which leads to the increase of the velocity difference inside and outside the passenger compartment and the increase of the shear force; In the figure on the right, due to the interference of the deflector and the rear-view mirror tail vortex on the free shear layer in the side window area, the shear layer is disturbed, resulting in higher speed in the vehicle. Therefore, the speed difference inside and outside the vehicle becomes smaller and the corresponding shear force becomes weaker.

Figure 13 shows that when the model of the diversion slice is added on the right figure, the distance between the free shear layer and the wake vortex of the mirror is obviously small. The rear view mirror tail vortex area has a stronger influence on the free shear layer.In addition to the rear-view mirror tail edge vortex area impact free shear layer and its vortex structure, the low-pressure region of the rear-view mirror tail vortex induces deflection in the free-shear layer, and the deflection-induced rear-view mirror tail vortex region is transient pulsation, this additional external influence has a greater disturbance on the trajectory of the free shear layer, which directly affects the development and movement of the free shear layer vortex.The free shear layer further deviates from the opening area of the side window. And the shear layer is "lifted up". The unstable vortex formed by the shear layer is away from the outside of the B-pillar or hits the B-pillar. Thus, that part of the vortex energy does not enter the cavity. This phenomenon is an important reason for buffeting noise reduction.

Forest Chemicals Revew
www.forestchemicalsreview.com
ISSN: 1520-0191
July-August 2021 Page No. 728-746
Article History: Received: 12 May 2021 Revised: 25 June 2021 Accepted: 22 July 2021 Publication: 31 August 2021

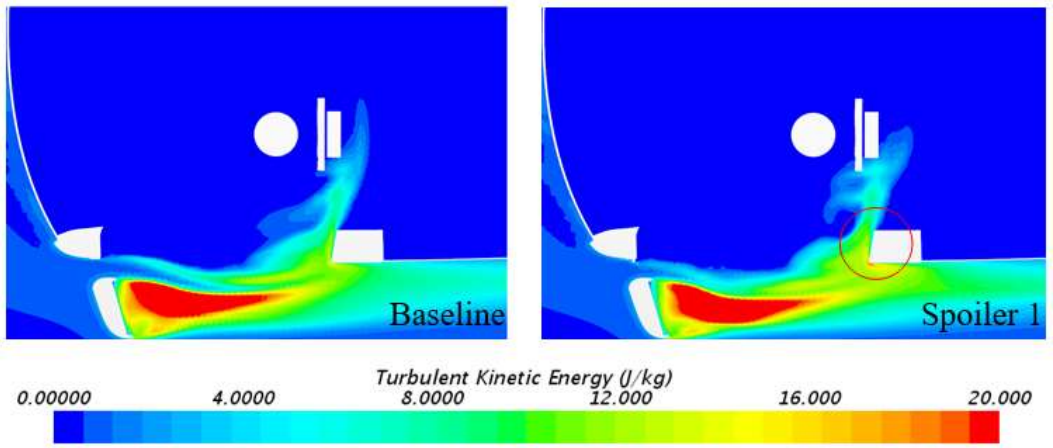

Fig 14: comparison of Z=0.7m plane kinetic energy cloud

The intensity of velocity pulsation in the flow field determines the size of aerodynamic noise. The magnitude of the turbulent kinetic energy can be used to measure the magnitude of the pulsation in the flow field, which in turn can determine the strength of the sound source. The right side of Figure 14 is the model with an added spoiler . The turbulent kinetic energy cloud shows that the model has a strong turbulent kinetic energy at the B-pillar. As the shear layer is lifted, the vortex strongly hits the B-pillar region, which is the main area where the broadband noise is generated. This phenomenon causes the left-side monitoring point to have a higher SPL (within 250 Hz) in the SPL curve (Figure 12).

5.2 Addition of Oblique Diversion Slice

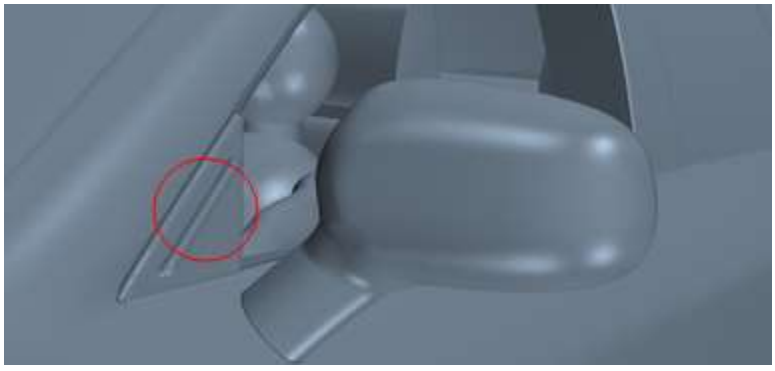

Fig 15: a oblique backflow slice to the position of the triangular window

In the position of the triangular window, adding oblique diversion slice as shown in Figure 15, the simulation results are as follows.

Forest Chemicals Revew
www.forestchemicalsreview.com
ISSN: 1520-0191
July-August 2021 Page No. 728-746
Article History: Received: 12 May 2021 Revised: 25 June 2021 Accepted: 22 July 2021 Publication: 31 August 2021

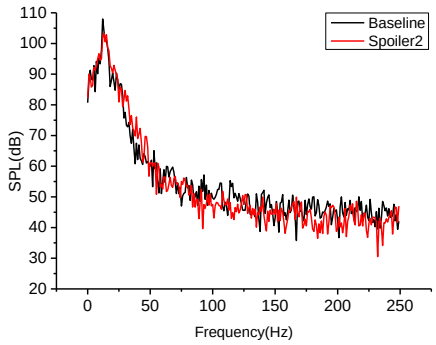

Figure 16: SPL of left rear monitoring point

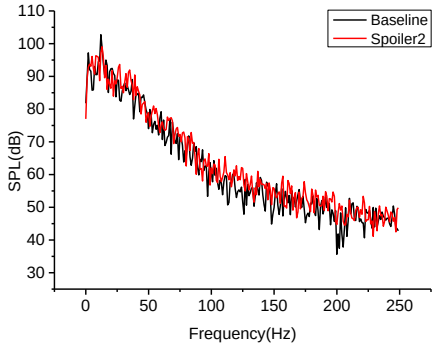

Figure 17: SPL of Left front monitoring point

In the case of the opening of the left front window (Figures 16 and 17), the addition of an oblique diversion slice has a significant restraining effect on the buffeting noise in the vehicle. The maximum noise reduction on the left rear side window can reach 4.7 dB, and the left front monitoring point can reduce the noise by 3.7 dB. These values show evident noise reduction. By comparing Figure 12 and Figure 17, it can be found that the broadband noise (within 250 Hz) at the left front monitoring point of the oblique diversion slice is lower than that of the vertical diversion slice.

Forest Chemicals Revew
www.forestchemicalsreview.com
ISSN: 1520-0191
July-August 2021 Page No. 728-746
Article History: Received: 12 May 2021 Revised: 25 June 2021 Accepted: 22 July 2021 Publication: 31 August 2021

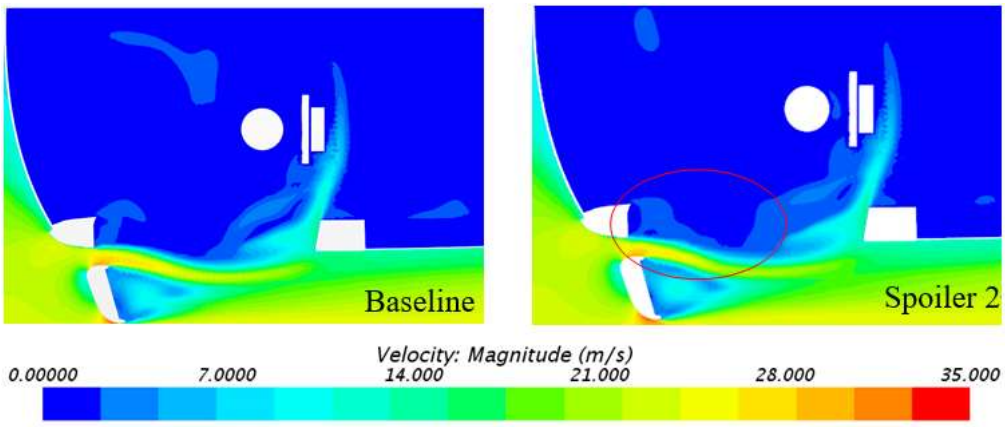

Fig 18: comparison of scalar plots of Z=0.7m plane velocity

Figure 18 shows that the principle of noise reduction using the oblique deflector is the same as that using a vertical deflector. However, the degree of deflection of the free shear layer toward the rear-view mirror is smaller than that of the vertical deflector. This phenomenon indicates that the effect of the mirror wake vortex on the free shear layer is reduced. However, the effects of the two control methods are equivalent. The oblique deflector guides part of the airflow upward along the A-pillar, thereby weakening the airflow energy in the triangular window region and simultaneously affecting the free shear layer in the A-pillar region.

VI. CONCLUSION

When the front side window is opened, there is serious buffeting noise in the cab. The large eddy simulation method can accurately solve the wind-induced vibration noise of automobile side window with high accuracy.

The self-excited oscillation of the shear layer, the periodic shedding and impact of the vortex, and the exchange of gas inside and outside the cavity eventually lead to complex pressure pulsation in the cavity. This is the main cause of wind vibration noise. It is found that the rear-view mirror tail vortex interacts with the free shear layer in the side window area, which has a greater impact on the buffeting noise level in the cab.

For the buffeting noise of the front side window, installing a vertical diversion slice with less influence on the external shape on the side of the triangular window results in the maximum drop of buffeting noise in the side window by 4.8 dB. The oblique deflectors produce a maximum noise reduction of 4.7 dB and effectively suppress broadband noise.

REFERENCES

Forest Chemicals Revew
www.forestchemicalsreview.com
ISSN: 1520-0191
July-August 2021 Page No. 728-746
Article History: Received: 12 May 2021 Revised: 25 June 2021 Accepted: 22 July 2021 Publication: 31 August 2021

[1] Gu ZQ, Xiao ZY, Mo ZJ (2007) Review of CFD Simulation on Vehicle Wind Buffeting. Noise and Vibration Control 27(4):65-68
[2] Cao F (2003) The Study Testing and Control for Coach Interior Noise. Chongqing University
[3] Hu XJ (2014) Automobile Aerodynamics. China Communications Press
[4] Zhang R (2014) Research on Human Ear Preesure Comfort during Door Closure of Passenger Car. Jilin University
[5] Didyk L A, Dirckx JJJ, Bogdanov VB et al. (2007) The mechanical reaction of the pars flaccida of the eardrum to rapid air pressure oscillations modeling different levels of atmospheric disturbances. Hearing Research 223(1):20-28
[6] Bodger WK, Jones CM (1964) Aerodynamic Wind Throb in Passenger Cars// SAE World Congress & Exhibition
[7] Huang L (2009) Study of Sunroof Buffeting Noise of Automobiles due to Wind Load. Noise and Vibration Control 29(2):38-41
[8] Kang N, Wang XC (2010) Influence of sunroof on flow field and aerodynamic noise inside the passenger compartment of the car. Journal of Aerospace Power 25(2):354-358
[9] Wang YP, Gu ZQ, Yang X et al. (2010) Numerical Simulation and Control of Automobile Sunroof Buffeting Noise. China Journal of Highway and Transport 23(6):108-114
[10] Hu YT, Xue YF, Chen J et al. (2011) Numerical Simulation and Experimental Study of Vehicle Aerodynamic Noise from Open Sunroof. Journal of Engineering Thermophysics 32(4):589-592
[11] Wang YP, Gu ZQ, Yang X (2012) Side window wind buffeting characteristics and reductions. Acta Aerodynamica Sinica 30(3):277-283
[12] Chen ZF, Wen GL, Li WP (2013) Influence of Stream Velocity on the Buffeting Characteristic of Vehicle Sunroof. Automobile Engineering 35(7):654-659
[13] Balasubramanian G, Mutnuri L A R, Sugiyama Z et al. (2013) A Computational Process for Early Stage Assessment of Automotive Buffeting and Wind Noise 6(2):1231-1238
[14] Yang Zhen Dong, Gu Zhen Qi, Dong GP et al. (2014) Analysis and optimal control for car sunroof buffeting noise. Journal of Vibration and Shock 33(21):193-201
[15] Oettle N, Bissell A, Senthooran S, et al. (2015) Assessment of Broadband Noise Generated by a Vehicle Sunroof at Different Flow Conditions using a Digital Wind Tunnel 8(3)
[16] Sinha S, Kavarana F, Dan W et al. (2016) A High Performance Airfoil-Profile Deflector for Open Sunroof Wind Noise// International Styrian Noise, Vibration & Harshness Congress: the European Automotive Noise Conference
[17] Zhang QD (2017) Wind Buffeting Noise Research on Side-window Combinaion under High Speed. Hunan University
[18] Chen Qing Bin (2019) Research and Optimization of Buffeting Suppression Measures for Passenger Cars. Shi Jiazhuang Tiedao University
[19] Dunai L, Lengua I, Iglesias M et al. (2019) Buffeting-Noise Evaluation in Passenger Vehicle BMV 530d. Acoustical Physics 65(5): 578-582
[20] Chen Z, Gu Z, Wang Z (2019) Research on the simplified vehicle window buffeting noise with a modified LRN CLES model using a transition-code based method. International Journal of Numerical Methods for Heat & Fluid Flow 29(9): 3169-3191

Forest Chemicals Revew
www.forestchemicalsreview.com
ISSN: 1520-0191
July-August 2021 Page No. 728-746
Article History: Received: 12 May 2021 Revised: 25 June 2021 Accepted: 22 July 2021 Publication: 31 August 2021

[21] Yin S, Gu Z, Zong Y et al. (2019) Sound quality evaluation of automobile side-window buffeting noise based on large-eddy simulation. Journal of Low Frequency Noise, Vibration and Active Control 38(2): 207–223
[22] Zhang Q, He Y, Wang Y et al. (2020) Computational study on the passive control of sunroof buffeting using a sub-cavity. Applied Acoustics 159: 107097-107105
[23] Kim H, Hu Z, Thompson D (2020) Effect of cavity flow control on high-speed train pantograph and roof aerodynamic noise. Railway Engineering Science 28(1): 54-74
[24] Wang Q, Chen X, Zhang Y (2021) An Overview of Automotive Wind Noise and Buffeting Active Control. SAE International Journal of Vehicle Dynamics, Stability, and NVH 5(4): 1-16
[25] Tang R, He H, Lu Z et al. (2021) Control of Sunroof Buffeting Noise by Optimizing the Flow Field Characteristics of a Commercial Vehicle. Processes 9(6): 1052
[26] Li S, Lu Z, Tang R et al. (2021) Optimization of wind resistance in commercial vehicles with consideration of sunroof buffeting noise. AIP Advances 11(8): 085304
[27] Yu A, Yi Y, Gu Z, et al. (2021) Research on wind buffeting noise characteristics of a vehicle based on ILRN and DES-ILRN method. Proceedings of the Institution of Mechanical Engineers. Part D, Journal of automobile engineering 235(1): 114-127
[28] Zhang Y, Hu X, Lan W, et al. (2021) Application of Omega vortex identification method in cavity buffeting noise. Journal of Hydrodynamics 33(2): 259–270
[29] Zhang YC (2011) Automotive aerodynamics numerical simulation technology. Peking University Press
[30] Wang FJ (2004) Analysis of Computational Fluid Dynamics. Tsinghua University Press
[31] Zhang Q (2012) Aeroacoustics basics. National defense industry press